[Research Paper] 대한금속 · 재료학회지 (*Korean J. Met. Mater.*), Vol. 61, No. 2 (2023) pp.120-125
DOI: 10.3365/KJMM.2023.61.2.120

Thermal and Mechanical Properties of Cu-Graphite Composites with Spatial Anisotropy

Geon Hong Ryu[1,†], Changil Son[2,†], Jeffrey C. Suhling[3], Jiseok Lee[2], Sangha Park[4,*], and Myunghwan Byun[1,*]

[1]*Department of Materials Engineering, Keimyung University, Daegu 42601, Republic of Korea*
[2]*School of Energy and Chemical Engineering, Ulsan National Institute of Science and Technology (UNIST), Ulsan 44919, Republic of Korea*
[3]*Department of Mechanical Engineering, Auburn University, AL 36849-5341, USA*
[4]*Daegu Mechatronics & Materials Institute (DMI), Daegu 42715, Republic of Korea*

Abstract: In the present study, we analyzed the thermal and mechanical properties of Cu-graphite composites (CGCs) with spatially anisotropic graphite layers. These composites were fabricated using a combination of electroless plating and spark plasma sintering (SPS) processes. Thermal conductivities and thermal expansion coefficients of the composites were measured using differential thermal analysis (DTA) and a laser flash method. In particular, the thermal expansion coefficients of the composites were investigated by comparative analysis, which was conducted by processing prototypes in a vertical direction with a parallel sector in the direction of the upper and lower axial pressure. The Cu reinforced with the graphite flake showed better thermal properties compared to the graphite fiber, while the graphite fiber led to better mechanical properties. This investigation was conducted to better understand the dependence of thermal properties on the morphologies of the graphite layers (i.e., flake and fiber types) in the Cu matrix. The bending strength and friction coefficient of the composites were also investigated. Taken together, the results from this work offer fruitful, yet practical information to utilize the CGCs as a thermal management material, essential for electric and electronic devices.

(Received 2 June, 2022; Accepted 11 November, 2022)

Keywords: Cu-graphite composite, spatial anisotropy, thermal and mechanical properties, spark plasma sintering

1. Introduction

For the past few decades, metal matrix-graphite composites have attracted considerable attention because of their excellent electrical conductivity, thermal conductivity, and friction resistance [1]. Among them, copper (Cu)-graphite composites could provide improved thermal and mechanical properties, which are crucial in low voltage and high current density electric and electronic devices [1-4]. Various techniques have been used to fabricate Cu-graphite composite systems, including hot pressing [5-7], vacuum pressure infiltration [8,9], electro- and electroless plating [10-13], chemical vapor deposition [14], spark plasma sintering [15,16], etc. Cu composites which incorporate thermally conductive graphite fillers provide advantages in weight reduction, by adding a large amount of graphite fillers makes pretreatment and post-processing essential, to establish heat conduction paths within the matrix [17]. It is very crucial that the composite system has excellent thermal conductivity, which means controlling variables so that heat can pass effectively (i.e., securing the passage of phonons as much as possible).

In the present paper, the thermal and mechanical properties of Cu composites reinforced with two types of graphite (fiber and flake) were investigated based on the pressing direction during the spark plasma sintering process. The spatial distribution of graphite fillers in the Cu matrix can be affected by sintering process conditions, thus triggering

[†]These authors contributed equally to this work.
- 류건홍: 석사과정, 손창일: 박사과정, Jeffrey C. Suhling · 이지석 · 박상하 · 변명환: 교수
**Corresponding Author:* Myunghwan Byun
[Tel: +82-10-4045-2496, E-mail: myunghbyun@kmu.ac.kr]
**Corresponding Author:* Sangha Park
[Tel: +82-10-3573-6533, E-mail: shpark@dmi.re.kr]

changes in thermal and mechanical properties.

The thermal conductivities and thermal expansion coefficients of the prepared composites were measured using differential thermal analysis (DTA) and a laser flash method. In particular, the thermal expansion coefficients of the composites were investigated by comparative analysis, conducted by processing prototypes in a vertical direction with a parallel sector in the direction of the upper and lower axial pressure. This investigation was conducted to help develop a rational understanding of the dependence of thermal properties on the morphologies of graphite layers (i.e., flake and fiber types) in the Cu matrix. The bending strength and friction coefficient of the composite were also investigated.

2. EXPERIMENTAL PROCEDURES

2.1 Preparation of Cu-graphite Composite Powders

Graphite (fiber and flake types, density of ~2.2 g/cm^3, Qingdao Krofmuehl Graphite Co., Ltd.) was chosen as the reinforcement filler. The mean sizes of the fiber and the flake type graphite were measured to be 80 μm and 120 μm, respectively. The whole surface of the graphite fiber and flake was coated with Cu by electroless plating followed by thermal handling at the elevated temperature of 380 °C in air for 60 min to activate the surface, and by ultra-sonication in acetic acid (CH_3CO_2H). In more detail, the electroless plating condition to achieve a 2 μm thick Cu coating on the graphite powders was an aqueous solution of 70 wt.% cupric sulfate pentahydrate ($CuSO_4 \cdot 5H_2O$) and 10 wt.% formaldehyde (HCHO) at 45 °C with pH values of 8–11 (tuned with varying content of NaOH). Representative field-emission scanning electron microscope (FE-SEM) images of the powders before sintering showed that the Cu coating covered the entire surface of each graphite particle, as shown in Fig. 1(b) and (d).

2.2 Spark Plasma Sintering

To consolidate the copper-coated graphite samples, the samples were first loaded into a rectangular graphite die (inner diameter of 40 mm × 40 mm) and then thermally treated by spark plasma sintering (SPS-3.20MK-V, Dr. Sinter Co., Ltd., Japan) under controlled conditions with a pressure of ~50 MPa and temperature ~920 °C. The resulting copper–graphite composites (CGCs) are shown in Fig. 1(c) and (e). The microstructures of the starting composite powders and the sintered composites were investigated using an X-ray diffractometer (XRD), a field-emission scanning electron microscope (FE-SEM), and high-resolution transmission electron microscope (HRTEM).

2.3 Tests for Thermal and Mechanical Properties

To examine the thermal properties of the CGCs, a rod type specimen was prepared with a diameter of 5 mm and length

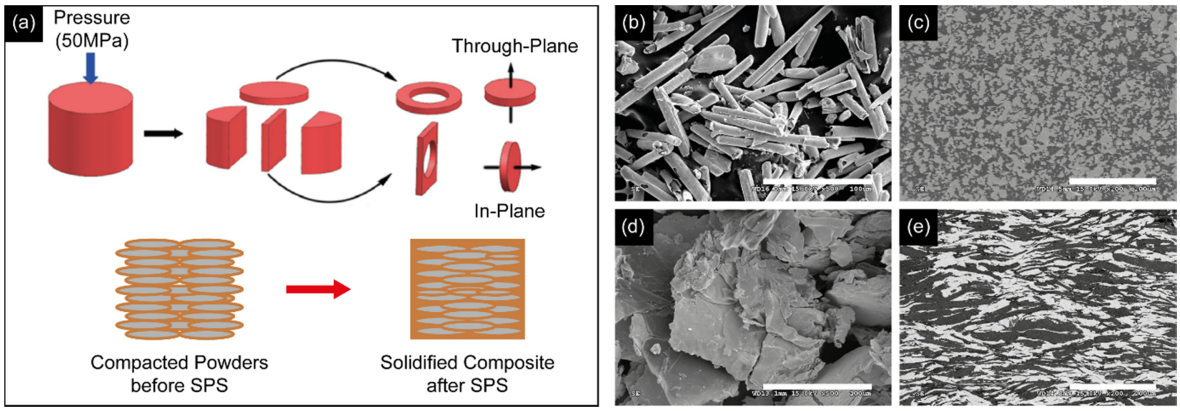

Fig. 1. (a) Upper panel: Schematic illustration showing the fabrication process of the Cu-graphite composites (CGCs), and the spatial distribution of the graphite fillers for different pressing directions (i.e., through-plane and in-plane). Lower panel: cartoons describing the CGC sample transition before and after the spark plasma sintering (SPS) process. (b) A representative field emission scanning electron microscope (FE-SEM) image of the fiber type graphite powders. (c) A representative FE-SEM image of the cross-section of the Cu reinforced with graphite fibers after the SPS process. Dark and bright areas are graphite and Cu, respectively. (d) A representative FE-SEM image of the flake type graphite powders. (e) A representative FE-SEM image of the cross-section of the Cu reinforced with graphite flakes after the SPS process. Dark and bright areas are graphite and Cu, respectively.

of 10 mm. The variation in thermal properties due to the spatial distribution of the graphite fillers (i.e., through- and in-plane) in the Cu matrix was also investigated, as schematically illustrated in Fig. 1(a). The bending strengths of the CGCs with 50, 60, and 70 vol.% of graphite were measured based on ASTM D790-10, the official standard methods for testing the flexural properties of unreinforced and reinforced plastics and electrical insulating materials. The friction coefficients of the CGCs with 50, 60, and 70 vol.% of graphite were measured based on ASTM D1894, the standard test methods for static and kinetic coefficients of friction of plastic film and sheeting. Thermal conductivity was measured by the laser flash method, which uses a specimen with a diameter of 10 mm × thickness 1 mm. To obtain the thermal diffusion coefficient, the front part of the specimen is heated while scanning a with a laser and measuring the heat radiated through the specimen, and the heat at the back of the specimen, using an infrared detector. Then, specific heat data was obtained using DTA and this data was used to calculate thermal conductivity.

3. RESULTS AND DISCUSSION

We first focused on characterizing the microstructures of the CGC before and after the SPS process. As clearly displayed in Fig. 2(a), very distinct peaks of the Cu phase were observed before and after the SPS process. The graphite peaks became much sharper after the sintering. The largest peak intensity was of the copper oxide phase. This is mainly due to a substantial reaction between the copper and atmospheric oxygen during the SPS process. Oxide formation can be inhibited if the SPS process is conducted in vacuum in the absence of oxygen. A FE-SEM investigation apparently shows the interfacial region of the Cu and the graphite phases (Fig. 2(b)). It is noteworthy that the formation of a graphite oxide phase in between the Cu and the graphite phases, as shown in Fig. 2(c). Graphite oxide is rationally considered to form during the SPS process and was firmly demonstrated in a previous study [16].

To further clarify the graphite oxide phases formed at the interfacial region between the Cu matrix and the graphite reinforcements, energy dispersive X-ray spectroscopy (EDS) was conducted on the sample, as shown in Fig. 3. This investigation revealed that the pristine graphite underwent a structural transition to graphite oxide, and to reduced graphite oxide during the SPS process. This phenomenon was also reported in previous studies of Cu-graphene nanocomposites [18-20]. It is worth noting, the thickness of the graphite oxide layer formed at the interface between the Cu matrix and the graphite was measured to be 4 to 6 nm.

The formation of the graphite oxide layer was observed for all experimental conditions with the flake-type graphite/Cu and the fiber-type graphite/Cu composites. Figure 4 represents the XPS results for the chemical composition and ionization etch depth at the interfacial area of the Cu-graphite composite. In all cases, the Cu and Cu_2O phases, and the composition of carbon, oxygen, and copper compounds, were investigated from a depth profile of 40 nm to the surface. Substantial compositional changes in carbon, oxygen, and copper compounds were observed at approximately 20 nm in

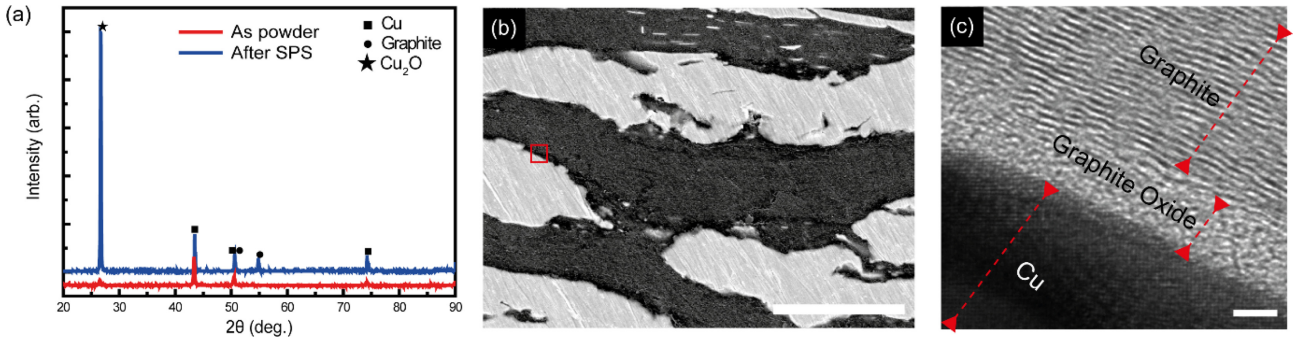

Fig. 2. (a) X-ray diffraction patterns of the CGC powders before and after the SPS process. (b) A representative FE-SEM image showing the interfacial region of the Cu and the flake-type graphite phases. The scale bar is 20 μm. (c) A representative High-resolution transmission electron microscope (HR-TEM) image of the interface between the Cu and the graphite phases corresponding to the red colored rectangular area in (b), confirming the formation of graphite oxide phase. The scale bar is 2 nm.

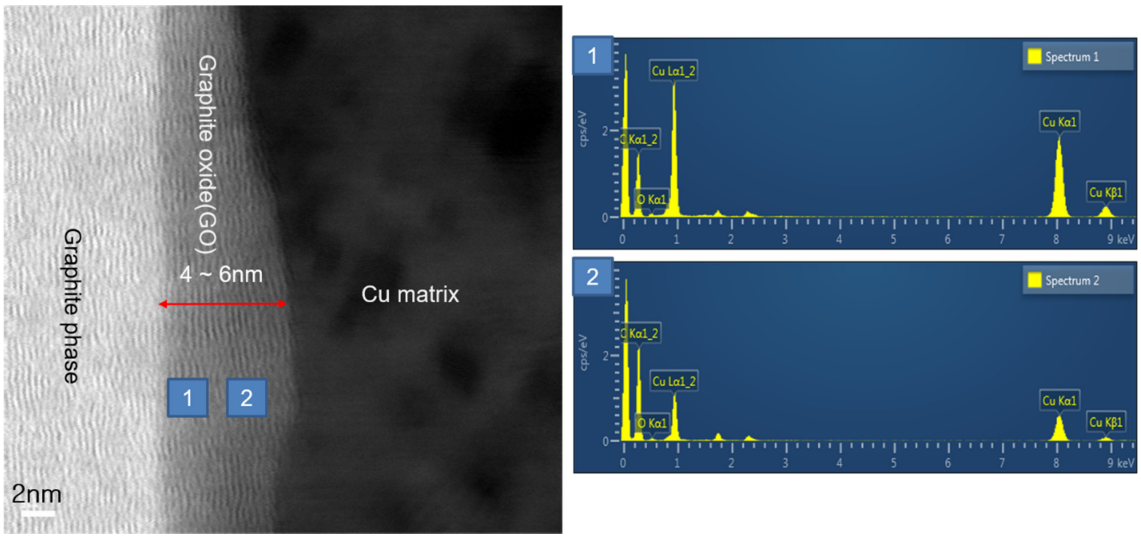

Fig. 3. EDS analysis of the CGCs. Left panel: High-resolution TEM image of the interface between the Cu matrix and the graphite reinforcements. Right panel: Energy dispersive X-ray spectra corresponding to the two selected regions of the Cu-graphite interface.

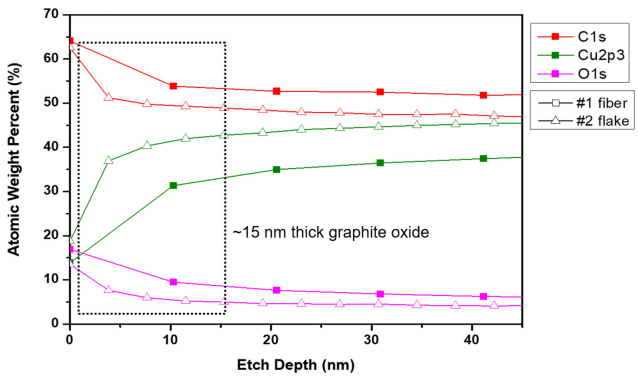

Fig. 4. X-ray photoelectron spectroscopy of the interfacial area between the Cu matrix and the graphite reinforcements.

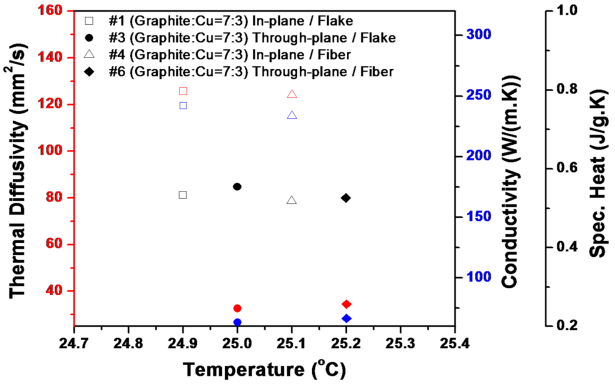

Fig. 5. Thermal properties of the CGCs with varying volume percentages of the graphite fillers, and spatial distribution of the graphite fillers at room temperature.

the depth direction from the surface of the composite, and the pure copper composition increased in weight. This strongly confirms the formation of rGO and GO phases in the anisotropic composite structure.

We then turned our attention to scrutinize the thermal properties of the CGCs with varying volume percentages of graphite fillers, both fiber and flake types, and their spatial arrangement. The choice of CGC was strongly motivated by the goal of preparing a thermal management composite material with a thermal expansion coefficient of 6.5–7.2 ppm/K, which is very similar to that of alumina.

Thermal properties including thermal diffusivity, thermal conductivity, and the specific heat of the CGCs were examined by varying the pressing direction of the samples (i.e., through-plane and in-plane) during the SPS process, and by changing the volume percentage of the graphite fillers, as shown in Fig. 5. Thermal diffusivity and conductivity were determined using the laser flash method, which is based on the temperature rise in a sample that is heated by a short laser pulse from one side. The specific heat was determined by differential thermal analysis (DTA), which is based on the difference in the temperature of the sample from the beginning and the end of the experiment, right after the temperature compensation. A CGC with 30 vol.% Cu and 70 vol.% graphite flake was prepared along the in-plane pressing direction, and it showed the largest value of thermal conductivity, of 250 W/m·K. Overall, the CGCs fabricated in the in-plane pressing direction showed thermal conductivities 4 times higher than those in the through-plane pressing

direction. When an anisotropic structure in the horizontal direction was formed, the composite material with the graphite flake shape showed a higher thermal conductivity value of 4–8 W/m·K than the graphite with a fiber shape. Based on the anisotropy of the thermal conductivity of the copper-graphite composite, it is thought that thermal energy conduction was more effective than the vertical interface because of the effect of the mean free path of phonons, and the heat transfer medium in the base.

The flexural strength of the CGCs was investigated for varying volume percentages of graphite fillers, sintered in the in-plane pressing direction, using a flexural tester as shown in Fig. 6. As the graphite content decreased, the flexural strength gradually increased. This variation in the flexural strength is deeply related to the graphite content and the interface area between the Cu and graphite phases. Over the entire content range, the composite samples reinforced with graphite fibers showed higher flexural strength values compared to those with flakes. This difference is presumably because the graphite flakes can more easily slide during bending deformation than the fibers [21]. This variation can also be explained by the following two feasible reasons. One is the interface region between the graphite and the Cu matrix, and the other is the surface area, which varied with type of graphite. For the flake-type, the interface area between the graphite and the Cu matrix has greater sliding motion on bending deformation, compared to the fiber-type. For the fiber-type, the surface areas of the Cu matrix and the graphite are much larger than with the flake-type. In Fig. 7, the friction coefficient of the CGC with 50 vol.% graphite flake is directly compared with Cu-Mo and Cu specimens. In the earliest stage, the CGC showed the largest friction coefficient value

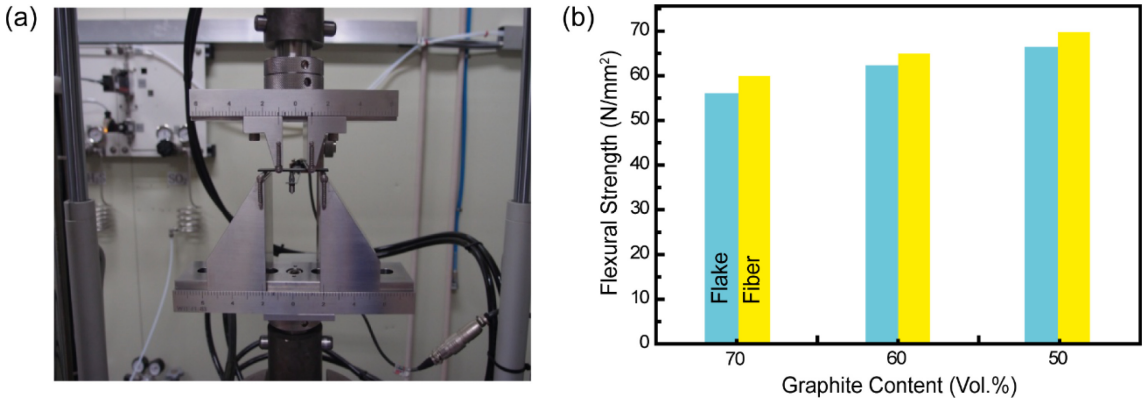

Fig. 6. Flexural (i.e., bending) strength of the CGCs with varying volume percentages of graphite filler. (a) A digital camera image of the flexural tester. (b) Flexural test results of the CGCs with varying volume percentages of the graphite filler. Blue and yellow bars indicate graphite flake and fiber, respectively.

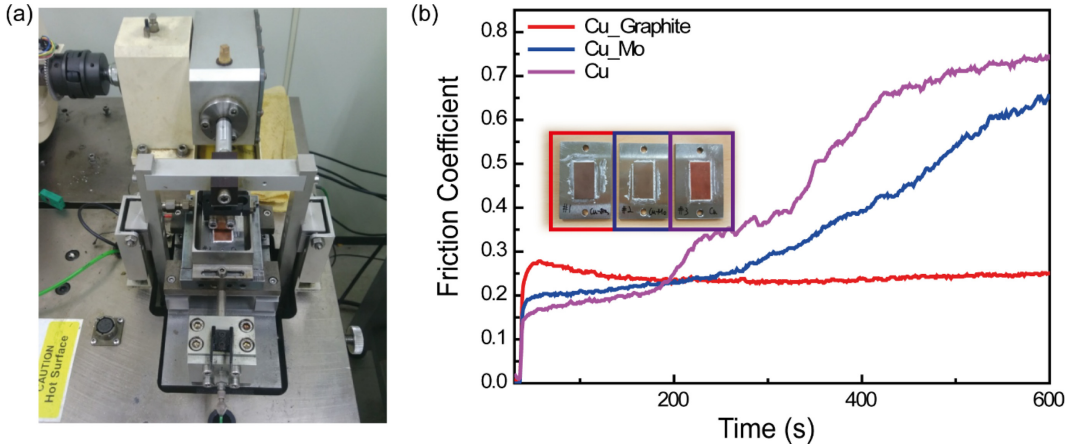

Fig. 7. Comparison of friction coefficient of the CGC with Cu-Mo and Cu specimens. (a) A digital camera image of the friction tester. (b) Plots of friction coefficients of the CGC, Cu-Mo, and Cu, respectively. Inset: Digital camera images of all samples.

compared to the Cu-Mo and Cu samples, but as the dwelling duration reached 200 s and further increased, an almost constant value appeared, which was much lower than the other samples. This is possibly due to the mechanical delamination of the graphite flakes from the Cu phases.

Since the Cu-Mo composites combine the low thermal expansion coefficient of Mo ($\alpha = 5.35\times10^{-6}$/K at room temperature) with the high thermal conductivity of Cu ($k = 401$ W/m·K at room temperature), this composite can be considered an interesting candidate for thermal management applications. Spatial anisotropy is assumed for the flake type. For the fiber type, the aspect ratio is not constant, and it was thought that it would be difficult to achieve consistent directionality of the fiber during the sintering process. However, with the fiber type, if the arrangement direction is perpendicular to the through-plane, that is, parallel to the in-plane during the sintering process, it is thought that a spatial anisotropic effect, like the flake type, can be obtained.

4. CONCLUSIONS

In brief, Cu-graphite composites (CGCs) with spatial anisotropy were successfully prepared using a combined process of electroless plating and spark plasma sintering. The structural evolution of the CGCs was fully investigated by XRD, FE-SEM, HRTEM, and XPS. To evaluate the practical uses of the CGCs, thermal and mechanical properties were characterized by the laser flash method, DTA, flexural testing, and scratch test. The Cu reinforced with the graphite flake showed better thermal properties than the graphite fiber, while the graphite fiber was observed to be better than the graphite flake for mechanical properties. The combination of results from this work are expected to provide fruitful, yet practical information for using CGCs as a thermal management material, which is essential for electric and electronic devices [22,23].

ACKNOWLEDGEMENT

This research was supported by the MOTIE (Ministry of Trade, Industry, and Energy) in Korea, under the Fostering Global Talents for Innovative Growth Program (P0008751) supervised by the Korea Institute for Advancement of Technology (KIAT).

REFERENCES

1. G. Z. Li, M. Yu, Z. L. Wang, J. Lin, R. S. Wang, and J. Fang, *J. Nanosci. Nanotechnol*. **6**, 1416 (2006).
2. J. Kováčik, Š. Emmer, J. Bielek, and L. Keleši, *Wear* **265**, 417 (2008).
3. L. Wu, Z. Zhao, P. Bai, W. Zhao, Y. Li, M. Liang, H. Liao, P. Huo, and J. Li, *Appl. Surf. Sci.* **503**, 144156 (2020).
4. K. Cheng, R. Liu, X. Xiang, X. Lin, and J. Chen, *Tribol. Lett.* **67**, 77 (2019).
5. R. Prieto, J. M. Molina, J. Narciso, and E. Louis, *Scripta Mater.* **59**, 11 (2008).
6. R. Shu, X. Jiang, Z. Shao, D. Sun, D. Zhu, and Z. Luo, *Powder Technol.* **349**, 59 (2019).
7. Q. Cui, C. Chen, C. Yu, T. Lu, H. Long, S. Yan, A. A. Volinsky, and J. Hao, *Carbon* **161**, 169 (2020).
8. Q. Kang, X. He, S. Ren, L. Zhang, M. Wu, T. Liu, Q. Liu, C. Guo, and X. Qu, *J. Mater. Sci.* **48**, 6133 (2013).
9. J.-H. Jang, H.-K. Park, J.-H. Lee, J.-W. Lim, and I.-H. Oh, *Compos. B. Eng.* **183**, 107735 (2020).
10. B. Jiang, H. Wang, G. Wen, E. Wang, X. Fang, G. Liu, and W. Zhou, *RSC Adv.* **6**, 25128 (2016).
11. K. Jagannadham, *J. Appl. Phys.* **110**, 074901 (2011).
12. K. Jagannadham, *Metall. Mater. Trans. B* **43**, 316 (2012).
13. Q. Liu, X.-B. He, S.-B. Ren, C. Zhang, L. Ting-Ting, and X.-H. Qu, *J. Alloy. Compd.* **587**, 255 (2014).
14. P. Goli, H. Ning, X. Li, C. Y. Lu, K. S. Novoselov, and A. A. Balandin, *Nano Lett.* **14**, 1497 (2014).
15. D.-D. Zhang and Z.-J. Zhan, *RSC Adv.* **6**, 52219 (2016).
16. M. Byun, D. Kim, K. Sung, J. Jung, Y.-S. Song, S. Park, and I. Son, *Appl. Sci.* **9**, 2853 (2019).
17. S. N. Leung, *Compos. B. Eng.* **150**, 78 (2018).
18. L. Wang, Y. Cui, B. Wei, S. Xu, J. Sheng, M. Wang, Y. Zhu, and W. Fei, *Sci. Rep.* **7**, 41896 (2017).
19. J. Hwang, T. Yoon, S.H. Jin, J. Lee, T.-S. Kim, S. H. Hong, and S. Jeon, *Adv. Mater.* **25**, 6724 (2013).
20. L. Wang, Y. Cui, B. Li, S. Yang, Z. Liu, R. Vajtai, and W. Fei, *RSC Adv.* **5**, 51193 (2015).
21. Y. Zhu, H. Bai, C. Xue, R. Zhou, Q. Xu, P. Tao, C. Wang, J. Wang, and N. Jiang, *RSC Adv.* **6**, 98190 (2016).
22. W.-S. Shin, S. Baek, and Y.-J. Kim, *Korean J. Met. Mater.* **60**, 471 (2022).
23. S. G. Jo, H.-I. Moon, Y. W. Kim, H. S. Dow, and J. W. Lee, *Korean J. Met. Mater.* **60**, 570 (2022).